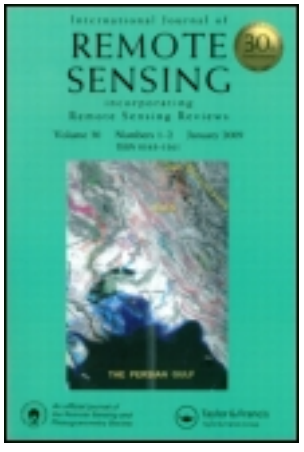


International Journal of Remote Sensing

Publication details, including instructions for authors and subscription information:
http://www.tandfonline.com/loi/tres20

# Monitoring soybean growth using L-, C-, and X-band scatterometer data

Yihyun Kim [a c], Thomas Jackson [b], Rajat Bindlish [b], Hoonyol Lee [c] & Sukyoung Hong [a]

[a] National Academy of Agricultural Science, Rural Development Administration, Suwon, Gyeonggi-do, 441-707, Republic of Korea

[b] USDA ARS Hydrology and Remote Sensing Laboratory, Beltsville, MD, 20705, USA

[c] Department of Geophysics, Kangwon National University, Hyoja-dong, Chuncheon, Gangwon-do, 200-701, Republic of Korea

To cite this article: Yihyun Kim , Thomas Jackson , Rajat Bindlish , Hoonyol Lee & Sukyoung Hong (2013): Monitoring soybean growth using L-, C-, and X-band scatterometer data, International Journal of Remote Sensing, 34:11, 4069-4082

To link to this article: http://dx.doi.org/10.1080/01431161.2013.772309

*International Journal of Remote Sensing*, 2013
Vol. 34, No. 11, 4069–4082, http://dx.doi.org/10.1080/01431161.2013.772309



# Monitoring soybean growth using L-, C-, and X-band scatterometer data

Yihyun Kim[a,c], Thomas Jackson[b]*, Rajat Bindlish[b], Hoonyol Lee[c], and Sukyoung Hong[a]

[a]*National Academy of Agricultural Science, Rural Development Administration, Suwon, Gyeonggi-do 441–707, Republic of Korea;* [b]*USDA ARS Hydrology and Remote Sensing Laboratory, Beltsville, MD 20705, USA;* [c]*Department of Geophysics, Kangwon National University, Hyoja-dong, Chuncheon, Gangwon-do 200–701, Republic of Korea*

(*Received 7 February 2012; accepted 11 January 2013*)

A ground-based fully polarimetric scatterometer operating at multiple frequencies was used to continuously monitor soybean growth over the course of a growing season. Polarimetric backscatter data at L-, C-, and X-bands were acquired every 10 min. We analysed the relationships between L-, C-, and X-band signatures, and biophysical measurements over the entire soybean growth period. Temporal changes in backscattering coefficients for all bands followed the patterns observed in the soybean growth measurements (leaf area index (LAI) and vegetation water content (VWC)). The difference between the backscattering coefficients for horizontally transmitted horizontally received (HH) and vertically transmitted vertically received (VV) polarizations at the L-band was apparent after the R2 stage (DOY 224) due to the double-bounce scattering effect. Results indicated that L-, C-, and X-band radar backscatter data can be used to detect different soybean growth stages. The results of correlation analyses between the backscattering coefficient for specific bands/polarizations and soybean growth data showed that L-band HH-polarization had the highest correlation with the vegetation parameters LAI ($r = 0.98$) and VWC ($r = 0.97$). Prediction equations for estimation of soybean growth parameters from the L-HH were developed. The results indicated that L-HH could be used for estimating the vegetation biophysical parameters considered here with high accuracy. These results provide a basis for developing a method to retrieve crop biophysical properties and guidance on the optimum microwave frequency and polarization necessary to monitor crop conditions. The results are directly applicable to systems such as the proposed NASA Soil Moisture Active Passive (SMAP) satellite.



## 1. Introduction

Soybean is a globally important crop that provides significantly more protein per acre than most other land uses and has health benefits such as cholesterol reduction. Remote sensing is an effective tool in monitoring soybean growth and yield assessment. Conventional visible and near-infrared remote-sensing techniques are widely used; however, they have limitations. Microwave remote sensing offers some potential improvements over conventional remote sensing due to its all-weather day-and-night imaging capabilities and because radar waves penetrate into the vegetation canopies. Previous studies have been carried out that attempted to estimate crop biophysical parameters using satellite-based synthetic

*Corresponding author. Email: thomas.jackson@ars.usda.gov

aperture radar (SAR) sensors. Plant parameters such as leaf area index (LAI), biomass, and plant height have been found to be correlated with backscattering coefficients and dependent on radar frequency and polarization (Ulaby et al. 1984; Bouman et al. 1991; Prevot et al. 1993; Kurosu, Fujita, and Chiba 1997; Pierce et al. 1998; Moran et al. 1998; Wigneron et al. 1999; Maity, Patnaik, and Panigraphy 2004; Chen, Lin, and Pei 2007; Cuizhen et al. 2009; Oh et al. 2009; Bouvet et al. 2011). However, crops are complex radar targets, and very few studies have examined radar responses over a full growth cycle.

Ground-based polarimetric scatterometer systems are very valuable in establishing basic relationships because both target and system parameters can be well controlled. An important advantage of these systems that can be exploited is the temporal observation of a specific crop target. Several articles have used this approach to explore relationships between backscattering coefficients and biophysical parameters. Inoue et al. (2002) investigated relationships between microwave backscatter signatures with rice canopy growth variables. Prasad (2011) studied soybean growth using a ground-based multitemporal, multiangle, and co-polarized X-band scatterometer data and found that LAI was correlated with the backscattering coefficient at an incidence angle of 40°.

Kim, Hong, and Lee (2009, 2010) suggested that the quality of a vegetation time series could be improved by the near continuous monitoring of the canopy. This approach allows the screening of data to reduce the impact of environmental effects caused by meteorological variables, in particular wind speed.

In this article, a ground-based fully polarimetric scatterometer operating at multiple frequencies (L-, C-, and X-bands) was used to continuously monitor the crop conditions of a soybean field. The system was set up to obtain data automatically every 10 min to provide observations of the diurnal patterns and, as noted earlier, to reduce noise due to meteorological factors. The polarimetric scatterometer components were installed inside an air-conditioned shelter to maintain constant temperature and humidity during the entire data acquisition period.

We analysed the relationships between L-, C-, and X-band signatures and biophysical measurements that included biomass, LAI, plant height, vegetation water content (VWC), and soil moisture over an entire soybean growth period. We then developed prediction equations for the retrieval of these soybean growth parameters from backscattering and evaluated their accuracy.

The results of this investigation offer new information that can be used to monitor and detect different soybean growth stages from scatterometer data. The results also show that L-band radar observations can be used to accurately retrieve VWC for soybeans. The experiment design and results are particularly relevant to the NASA Soil Moisture Active Passive (SMAP) satellite scheduled for launch in 2014.

## 2. Methods

### *2.1. Study site and soybean growth measurements*

This study was conducted at the National Institute of Crop Science (NICS) experimental field (Latitude, 37.2597° N; Longitude, 126.9757° E) located in Suwon, Korea, from June until October of 2010. The size of the soybean field was 25 m × 32 m, and the sowing date of soybean (*Glycine max L. Merrill*) was 4 June 2010. Plant spacing was 60 cm × 15 cm. The plants reached peak biomass on 28 September 2010 and were harvested on 20 October 2010 (139 days after sowing). Crop row orientation was the same as the direction of the microwave antenna beam, i.e. the relative azimuth angle was zero. Soil chemical properties of this study site are shown in Table 1. The soil texture in the field is classified as loam with on average 24.4% silt, 40.4% sand, 35.2% clay, and a measured bulk density of 1.26 g $cm^{-3}$.

Table 1. Soil chemical properties of the study site.

| | | | | Exchangeable cations | | | | | |
|---|---|---|---|---|---|---|---|---|---|
| pH | OM | $NH_4$–N | Available $P_2O_5$ | K | Ca | Mg | CEC | Bulk density | Soil texture |
| 1:5 | g $kg^{-1}$ | mg $kg^{-1}$ | mg $kg^{-1}$ | $cmol^+$ $kg^{-1}$ | | | $cmol^+$ $kg^{-1}$ | g $cm^{-3}$ | Loam |
| 5.9 | 18.3 | 9 | 173 | 0.3 | 5.3 | 2.0 | 12.7 | 1.26 | |

Note: OM, Organic Matter; CEC, Cation Exchange Capacity; $cmol^+$ $kg^{-1}$, centi-mol per kg.



Soybean biophysical measurements included fresh and dry weight, plant height, LAI, VWC, and pod weight. Measurements were made weekly using a destructive method. A total of 15 soybean samples were collected on each sampling date, and fresh weight was measured as the sum of all leaves, stem, and pods. Samples were then dried in an oven for 36 hours at 60 °C to determine the dry weight. VWC was derived by computing the difference between the fresh and dry weights. Leaves were detached from the stems, and the leaf area was measured using LAI-3100 (LI-COR, Lincoln, NE) to obtain the LAI by dividing the total leaf area by the area of the soybean cluster. Measurement of the soil moisture within the top 5 cm was performed using a portable probe (Echo-5 TE probe, Decagon Devices, Inc., Pullman, WA, USA).

Correlation and regression analyses between backscattering coefficients and growth data were conducted using SAS (Statistical Analysis System, Enterprise Guide ver. 4.2, SAS Institute Inc.). The null hypothesis of the correlation being zero was tested using the *t*-test with a confidence level of 0.05. The results are described in more detail in Table 3.

### 2.2. *Microwave scatterometer system*

The scatterometer system was installed inside a shelter at the edge of the soybean field prior to sowing (3 June 2010). The shelter was used to maintain constant instrument temperature and humidity over the entire acquisition period. The system consists of L-, C-, and X-band dual square horn antennas with dual-mode transducers, a vector network analyser (VNA, 20 MHz ∼ 20 GHz), radio frequency (RF) cables, an RF switch, and a computer that controls frequency, polarization, and data storage (Table 2, Figure 1). The sizes of

Table 2. Specification of the L-, C-, and X-band automatic scatterometer system.

| Parameters | | L-band | C-band | X-band |
|---|---|---|---|---|
| Frequency (GHz) | | 1.27 ± 0.06 | 5.3 ± 0.3 | 9.65 ± 0.5 |
| Beam width | E-plane (°) | 20 | 15 | 12 |
| | H-plane (°) | 20 | 15 | 13 |
| Number of frequency points | | 201 | 801 | 1601 |
| Antenna type | | | Dual polarimetric square horn | |
| Antenna gain (dB) | | 12.4 | 20.1 | 22.4 |
| Slant range resolution (m) | | 1.25 | 0.25 | 0.15 |
| Bandwidth (MHz) | | 120 | 600 | 1000 |
| Wavelength (m) | | 0.23 | 0.056 | 0.031 |
| Polarization | | | HH, HV, VH, VV | |
| Incident Angle (°) | | | 40 | |
| Platform height (m) | | | 4.16 | |
| Measurement interval | | | 10 min | |

Figure 1. Photographs of the automatic scatterometer system. The system was installed in a shelter with the X-, L-, and C-band antennas (from left to right) looking down the soybean field at 40° incidence angle (left). The RF system inside the shelter is composed of a notebook computer, a vector network analyser, a microwave switch, power unit, and an air conditioner (not shown here) (right).



the antenna footprints are 3.40 m × 2.44 m (L-band), 1.89 m × 1.42 m (C-band), and 1.50 m × 1.14 m (X-band).

This system automatically measured the fully polarimetric backscattering coefficients of the soybean field every 10 min using the RF switch for all three frequency bands. Providing a range of incidence angles was sacrificed, and a single fixed angle of 40° was used to avoid uncertainty associated with positioning, which was found in a previous study (Kim, Hong, and Lee 2009). The earlier investigation found that the best relationship between backscattering and crop growth parameters was at 40°.

The polarimetric scatterometer operates in a stepped-frequency sweep mode with all combinations of horizontal (H) and vertical (V) polarization. The range resolution ($R$) is determined by $\Delta R = c/2B$, where $c$ is the speed of light in free space and $B$ is the system bandwidth. The maximum range of the radar system is related to the maximum sampling number of the VNA and the range resolution via $R_{\max} = (N-1)\,\Delta R$, where $N$ is the number of frequency points. The polarimetric scatterometer provides the time domain radar return from a target for the fully polarimetric amplitude (HH, HV, VH, and VV) and phase data set. Backscattering coefficients ($\sigma^\circ$) are then calculated by applying the radar equation (Sarabandi, Oh, and Ulaby 1992). The system was calibrated using a triangular trihedral corner reflector with a backscattering coefficient of 0.7 dB. The noise background level was measured by pointing the antennas towards the sky. The level of white noise was −110 dB, −105 dB, and −100 dB for X-, C-, and L-bands, respectively. The power data were converted to $\sigma^\circ$ (dB) using the calibration data. A daily average backscattering coefficient was computed from the 144 measurements (every 10 min) obtained over the course of each day.

### *2.3. Pauli decomposition*

There are three different types of target decomposition methodologies that are based on: (1) Mueller and Stokes vector, (2) eigenvector analysis of the covariance matrix, and (3) coherent decomposition of the scattering matrix (Cloude and Pottier 1996). The observed polarimetric response from a target is a combination of coherent speckle noise and

scattering effects (from surface to volume). The main problem with coherent decomposition is that it ignores the speckle noise associated with radar observations. Here, backscatter observations over the field of view in the soybean field were averaged in order to reduce noise. Moreover, scatterometer observations made every 10 min were averaged to obtain a daily average backscatter coefficient. The aggregation of backscatter observations in space and time should greatly reduce the speckle noise. As a result, the coherent decomposition methodologies are the best option for this data set.

Coherent decomposition expresses the observed scattering $\boldsymbol{S}$ matrix as a combination of basic matrices corresponding to different scattering mechanisms. This approach is useful because it provides information on the dominant scattering mechanisms, which can be used for the purpose of classification or estimation of the geophysical parameters. It is possible that the decomposed components of scattering may provide information about the biophysical properties of the vegetation, such as density and height of the crop canopy. Coherent methodologies to decompose multipolarized scattering into components have been proposed in previous investigations. For example, Freeman and Durden (1992) suggested a three-component decomposition to estimate the volume, surface, and double-bounce scattering components, and Lee and Pottier (2009) proposed Pauli decomposition for scattering characters.

Pauli decomposition of polarimetric data is one of the simplest and intuitive methods to separate the backscatter into single bounce, double bounce, and volume scattering. Pauli decomposition of the scattering matrix is often employed to represent all the polarimetric information in a single SAR image. Given a measured scattering matrix $[\boldsymbol{S}]$, Pauli decomposition is described by the following equation (Lee and Pottier 2009):

$$[\boldsymbol{S}] = \begin{bmatrix} S_{hh} & S_{hv} \\ S_{hv} & S_{vv} \end{bmatrix} = \alpha[\boldsymbol{S}]_a + \beta[\boldsymbol{S}]_b + \gamma[\boldsymbol{S}]_c, \tag{1}$$

where $[\boldsymbol{S}]_a$, $[\boldsymbol{S}]_b$, $[\boldsymbol{S}]_c$ are the Pauli basis matrices. $\alpha$ represents single-bounce scattering, $\beta$ means double-bounce scattering, and $\gamma$ stands for volume scattering. The $\alpha$, $\beta$, and $\gamma$ can be computed by rearranging the terms as follows:

$$\alpha = \frac{S_{hh} + S_{vv}}{\sqrt{2}}, \tag{2}$$

$$\beta = \frac{S_{hh} - S_{vv}}{\sqrt{2}}, \tag{3}$$

and

$$\gamma = \sqrt{2}s_{hv}. \tag{4}$$

In the case of mature soybean plants, the radar signal is reflected from the top of the canopy and the single bounce dominates the backscatter signal. Double bounce occurs when a radar signal is reflected once by the soil surface and the vegetation canopy (stems or leaves). Volume scattering happens when the radar signal is able to penetrate through the crop canopy and is then scattered multiple times within the vegetation canopy. These scattering mechanisms are all dependent on the frequency, polarization, and incident angle.

## 3. Results and discussion

### 3.1. Temporal patterns of backscatter and soybean growth data

Figure 2 shows photographs of soybean at different growth stages during this investigation. Soybean growth stages are distinguished by plant development as either vegetative (V) or reproductive (R). The vegetative stages are numbered according to how many fully developed trifoliate leaves are present. Vegetative stages can be further subdivided into vegetative emergence (VE, A: DOY 166), vegetative cotyledon (VC, B: DOY 173), vegetative first trifoloioate (V1, C: DOY 179), and vegetative ninth trifoloioate (V9, D: DOY 200). The reproductive stages begin at flowering and include pod development, seed development, and plant maturation. Reproductive stages are subdivided into beginning bloom (R1, E: DOY 214), full bloom (R2, F: DOY 224), beginning pod (R3, G: DOY 228), full pod (R4, H: DOY 242), beginning seed (R5, I: DOY 249), full seed (R6, J: DOY 277), beginning maturity (R7, K: DOY 280), and full maturity (R8, L: DOY 287).

Figure 3 shows the temporal patterns of the soybean growth parameters over the study period. LAI, fresh weight, plant height, and VWC increased as growth advanced, reached a maximum on DOY 271, and then decreased. Pod weight increased until R6 stage (J, DOY 277) and decreased afterwards.

Figure 4 shows the observed L-, C-, X-band $\sigma^\circ$ for all polarizations. The backscatter coefficients decrease with an increase in frequency. L-band backscattering coefficients were larger than those observed using C- or X-band during the investigation. Backscattering coefficients for all frequencies and polarizations increased until DOY 271 and then

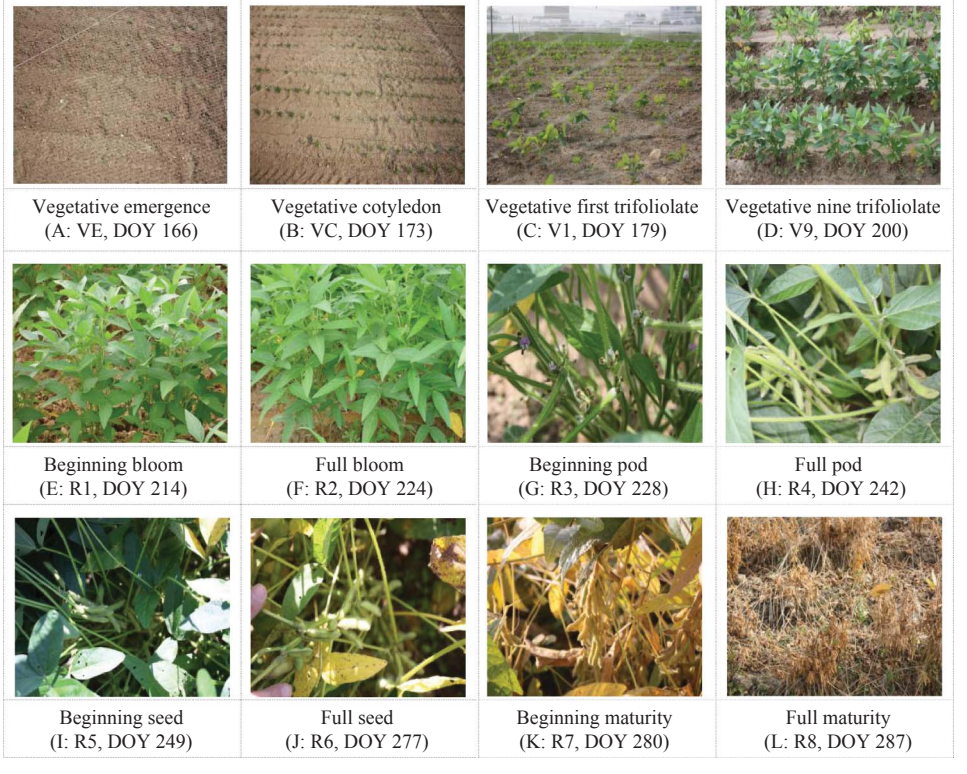


Figure 2. Field photographs of soybean in various growth stages.

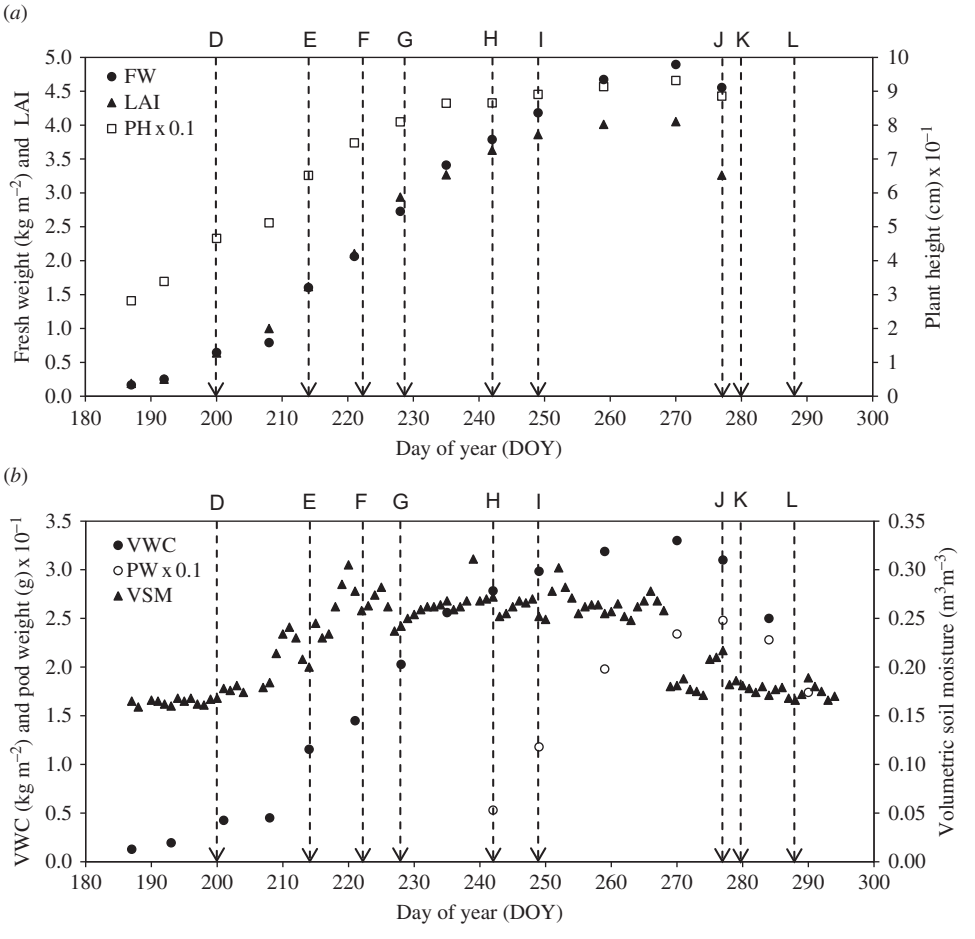


Figure 3. Temporal variations of soybean growth biophysical variables: (*a*) fresh weight (FW), LAI, and plant height; (*b*) vegetation water content (VWC), pod weight (PW), and volumetric soil moisture (VSM). Letter codes are described in Figure 2.

decreased along with LAI, fresh weight, plant height, and VWC. VV-polarization backscattering coefficients were higher than HH- or HV-polarization during the early growth period (DOY 155 – DOY 199). HH-polarization backscattering coefficients were higher than the other polarizations after the V9 stage (D, DOY 200) for the L-band (Figure 4(*a*)). The difference between the backscattering coefficients for HH- and VV-polarizations at the L-band was larger after the R2 stage (F, DOY 224), which lasted until the harvesting stage (DOY 294).

Changes in the C-band backscattering coefficients over the study period are shown in Figure 4(*b*). HH-polarization backscattering coefficients became higher than VV-polarization on DOY 212, which is near the R1 stage (E, DOY 214). The range of backscattering coefficients reached a maximum on DOY 271 and then rapidly decreased. The range of backscatter for the X-band was lower than for the L- and C-bands. The difference in $\sigma^\circ$ between HH- polarization and VV-polarization was lower than the other bands over the entire growth stage (Figure 4(*c*)). Our interpretation of the results is that the HH-backscattering coefficient is higher than VV at the L-band due to canopy–ground

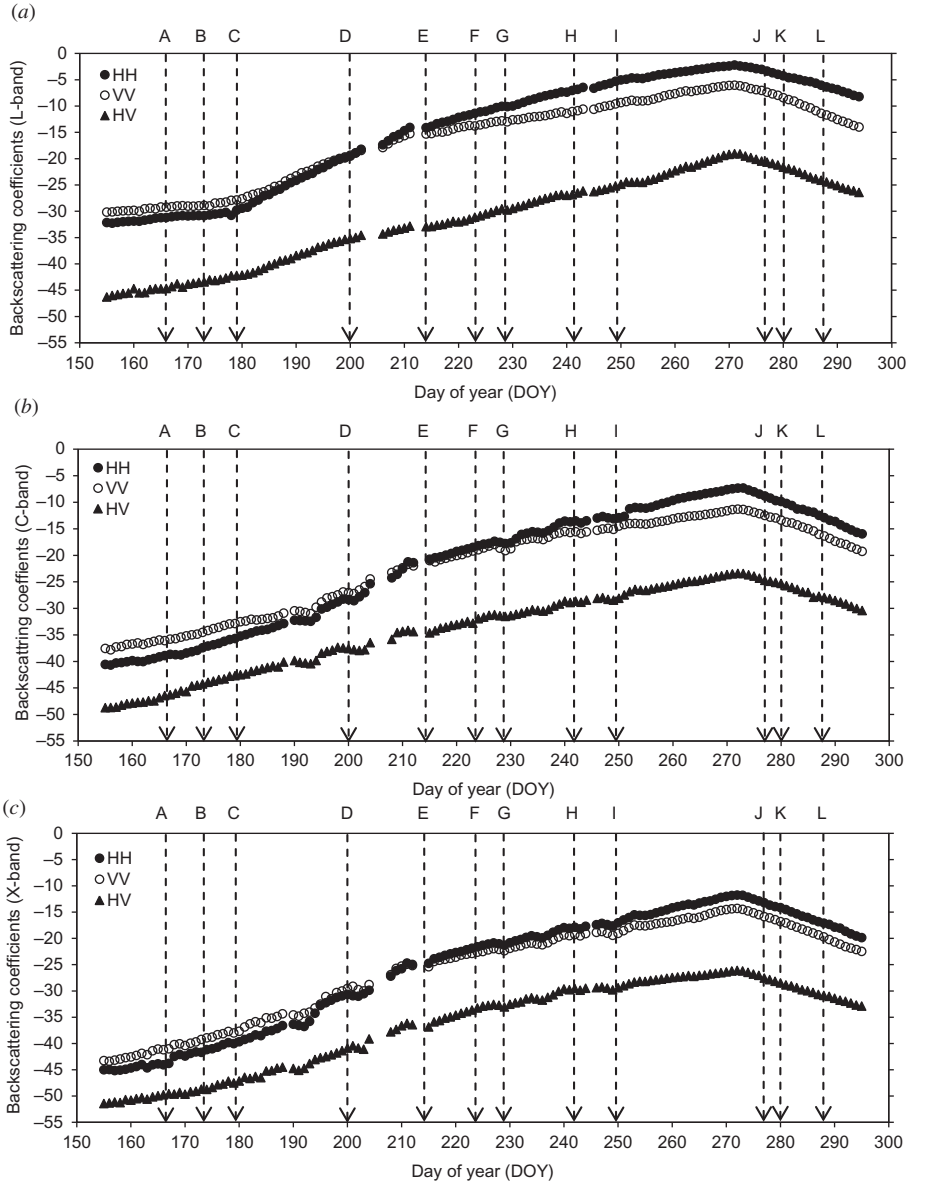


Figure 4. Temporal variations of HH, VV, and HV channels over the whole soybean growth period: (*a*) L-band, (*b*) C-band, and (*c*) X-band. Letter codes are described in Figure 2. Backscatter is expressed in units of dB.

interaction. The canopy–ground interaction decreases with an increase in frequency (smaller wavelength). At 9.6 GHz (X-band), the canopy–ground interaction is reduced. Thus, the VV and HH observations are closer to each other. The HV-backscatter is lower than the co-polarized (HH or VV) observations (X-band, ~7 dB; C-band, ~10 dB; and L-band, ~15 dB). The longer wavelengths are able to penetrate deeper into the vegetation canopy layer resulting in greater canopy–canopy interaction. The difference between

co-polarized observations (HH or VV) and cross-polarized observations increases with frequency as the soybean canopy–canopy interaction increases.

Figure 5 shows the Pauli decomposition of the backscattering coefficients for the three frequency bands. Single bounce ($\alpha$) is the dominant component over the entire study period for all bands, and the Pauli decomposition value was the highest for the L-band. Double bounce ($\beta$) becomes higher than volume scattering ($\gamma$) during the R2 stage (F, DOY 224) and the difference between the two components was more significant after the R4 stage (H, DOY 242) for the L-band (Figure 5(*a*)). Based upon these observations, we

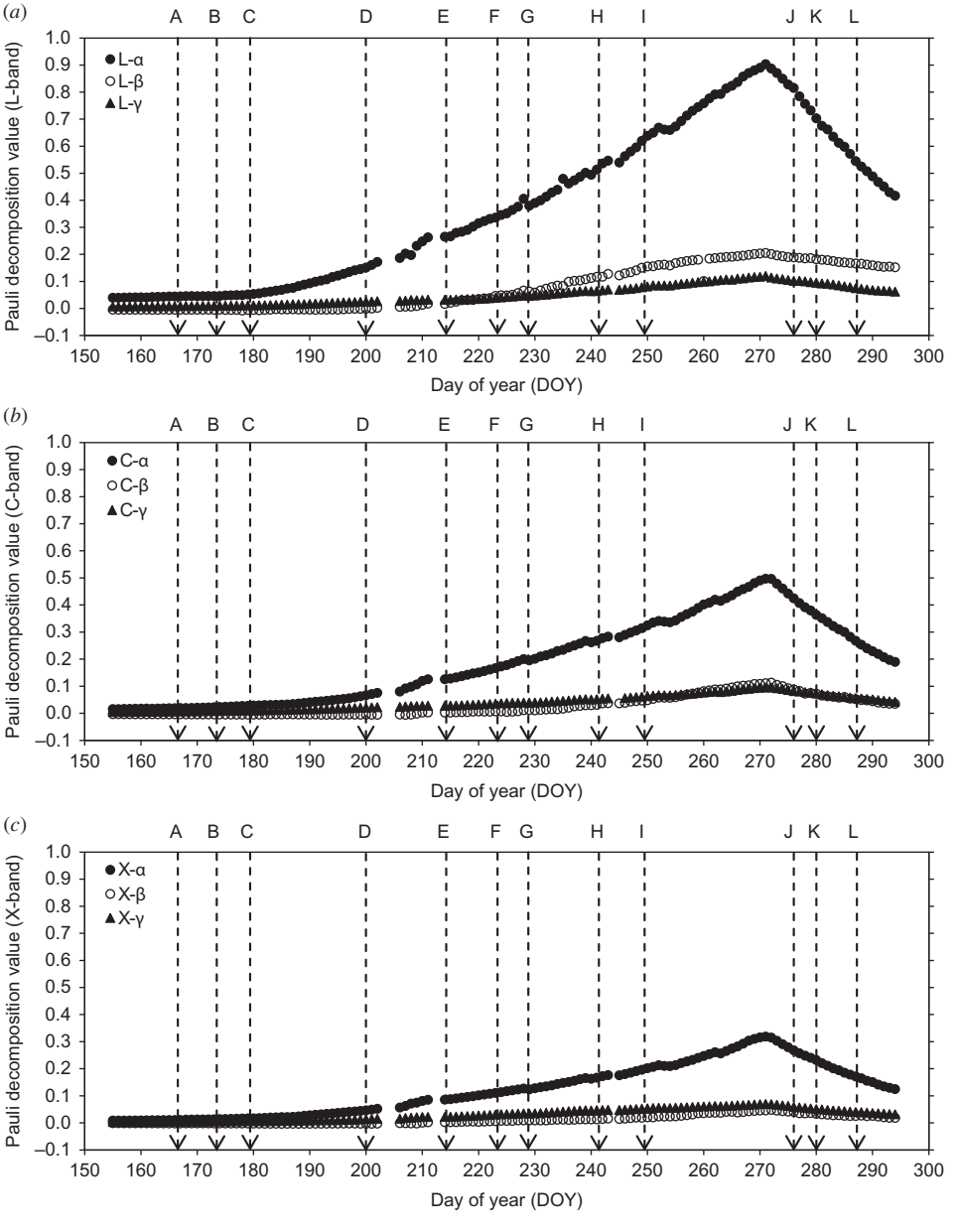


Figure 5. Components of Pauli decomposition ($\alpha$, $\beta$, and $\gamma$) in (*a*) L-band, (*b*) C-band, and (*c*) X-band.

concluded that the Pauli decomposition for the L-band was related to the double-bounce scattering. This result is attributed to the deeper penetration of longer wavelengths into the soybean canopy. Double-bounce and volume scattering were approximately equal for the C-band (Figure 5(*b*)), and volume scattering was higher than double bounce for the X-band (Figure 5(*c*)).

These results of the investigation indicate that different scattering mechanisms govern the radar response during different soybean stages. Vegetation substages (VE–V9) are not easy to detect using radar backscattering data. However, the results of this investigation indicate that L-, C-, or X-band radar backscatter data can be used to detect the beginning of the bloom (R1, E; DOY 214) and full bloom (R2, F: DOY 224) stages. The HH radar backscatter for the C- and X-bands became greater than the VV backscatter at the beginning of the bloom stage (HH > VV) (Figures 4(*b*)–(*c*)). At the start of the full bloom stage, the L-band double bounce was higher than the volume scattering (Figure 5(*a*)). At the start of the full bloom stage, the L-band double bounce was higher than the volume scattering (Figure 5(*a*)). It may be possible to exploit these unique characteristics of the radar backscatter to identify the different soybean growth stages. The maximum growth stage of soybean can also be detected using L-band double-bounce scattering. The peak of the double-bounce effect coincides with the peak of VWC on DOY 271.

### *3.2. Retrieval of growth parameters*

Table 3 summarizes the correlation coefficients for the backscattering coefficient for each band polarization and each of the measured biophysical variables. It also includes the results of the *t*-test for statistical significance of this correlation based upon sample size and a confidence level of 0.05. The backscattering coefficient is expected to be a function of physical parameters of the target such as structure and dielectric constant. L-HH $\sigma^\circ$ and LAI had a statistically significant correlation ($r = 0.98$). In addition, all of the other polarizations for the L- and C-bands also had statistically significant correlations ($r \geq 0.82$). However, the relationships between X-band options and LAI had lower correlations ($r = 0.74 - 0.78$) than those of the L- and C-bands. VWC and L-HH $\sigma^\circ$ had a statistically significant correlation ($r = 0.97$) and, as shown in Table 3, the other L- and C-band channels also had positive correlations.

The correlation coefficients were highest for L-band observations and lowest for the X-band. Also, HH-polarization had the highest correlations among the polarization channels (HH, VV, and HV). Our analysis focused on LAI and VWC because they are the most commonly used vegetation parameters in radar backscatter algorithms. However, similar results were also found for other measured vegetation parameters (fresh weight, plant height, and pod weight).

Table 3. Correlation coefficients for the relationship between the backscattering coefficients and biophysical properties over the entire study period.

| | L-band | | | C-band | | | X-band | | |
|---|---|---|---|---|---|---|---|---|---|
| Growth data | HH | VV | HV | HH | VV | HV | HH | VV | HV |
| Leaf area index | 0.98 | 0.94 | 0.91 | 0.84 | 0.83 | 0.82 | 0.78 | 0.77 | 0.74 |
| Vegetation water content | 0.97 | 0.94 | 0.90 | 0.85 | 0.86 | 0.83 | 0.77 | 0.76 | 0.74 |

Note: All values were found to be statistically significant using a *t*-test and a confidence level of 0.05 for the sample size of 15.

These results were also considered in the context of previous investigations. Brakke et al. (1981) examined Ku-band observations for varying polarizations and incidence angles and found that LAI had the best correlation with HH at 30° in wheat, corn, and sorghum. Inoue et al. (2002) utilized an automatic scatterometer system to obtain full polarimetric observations at five frequencies (Ku-, Ka-, X-, C-, and L-bands) nine times per day. They found that C-band backscattering (incidence angle of 25° for HH- and HV-polarization and incidence angle of 35° for HV-polarization) had the highest correlation with LAI for rice ($r = 0.96 – 0.97$). However, in a previous experiment by Kim, Hong, and Lee (2009) involving varying incidence angles, HH- and VV-backscattering coefficients at lower incidence angles (≤35°) had lower correlation with LAI. Several researchers (Wigneron et al. 1999; Picard, Le Toan, and Mattia 2003; Singh 2006) have also found strong interaction with the LAI and fresh biomass at an incidence angle of 40° for crops that include wheat, rice, soybean, and sunflower. These differences between experimental results may be due to variations in crop structure, weather conditions, crop types, and system parameters.

Volumetric soil moisture (VSM) was measured during the experiment; however, due to meteorological conditions, its temporal variations closely match the vegetation growth pattern (see Figure 3(*b*)). The correlations of VSM with VWC and LAI were 0.65 and 0.77, respectively. As shown in Table 3, the correlations of backscatter (L-HH) with VWC and LAI were close to 1. The largest value of the correlation of backscatter (L-HH) with soil moisture was 0.5. A closer examination of Figures 3(*b*) and 4(*a*) indicates that both backscatter and vegetation growth exhibit very consistent temporal patterns. Soil moisture has the same general trends but also exhibits some large deviations on a day-to-day basis, which are not reflected in the backscatter. Based upon this information, we concluded that backscatter was responding to changes associated with vegetation growth and not to VSM. The soil moisture effect on backscatter cannot be detected for this set of experimental conditions.

Based on the observed relationships between the backscattering coefficients of three bands/polarizations and biophysical variables, prediction equations were developed using the L-band HH-polarization backscattering data. Root mean square error (RMSE) was used as a metric for assessing retrieval performance.

Figure 6 shows the relationship between L-HH $\sigma^\circ$ and the two soybean growth parameters (LAI and VWC). As expected from the correlation analysis, the L-HH $\sigma^\circ$ has a strong

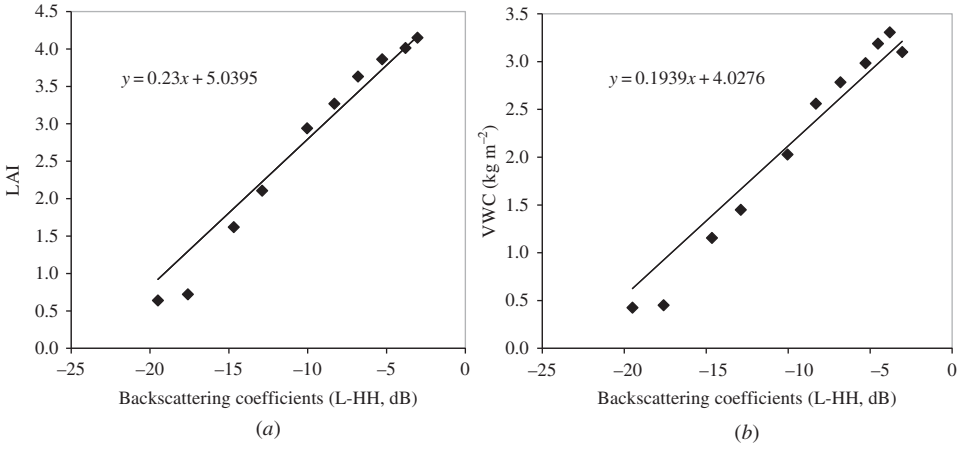


Figure 6. Relationship between backscattering coefficients (L-band HH-polarization) and soybean growth parameters: (*a*) LAI and (*b*) vegetation water content (VWC).

Table 4. Statistical performance of soybean growth retrievals using regression equations based on L-band backscattering coefficients.

| $y$ | $x$ | Regression equation | RMSE |
|---|---|---|---|
| Leaf area index | L-HH | $y = 0.23x + 5.0395$ | 0.1045 |
| Vegetation water content | L-HH | $y = 0.1939x + 4.0276$ | 0.0796 kg m$^{-2}$ |

Note: The backscattering coefficient is expressed in units of dB.



linear relation with LAI and VWC. The accuracy of the LAI retrievals as measured by the RMSE was 0.1045 (Table 4). The RMSE of the VWC estimated using L-HH observations was 0.0796 kg m$^{-2}$. The performance of both prediction equations is considered to be very good.

We found that the soybean growth stage can be predicted using this ground-based scatterometer based on the double-bounce effect. L-band $\sigma^\circ$ has a strong relationship with both LAI and VWC and as a result it was possible to develop retrieval equations for estimating LAI and VWC using the backscatter data. These results demonstrate the potential of using L-band radar observations from the upcoming SMAP satellite mission to determine growth variables and soil moisture information and contribute to crop growth monitoring.

## 4. Conclusions

A ground-based multifrequency (L-, C-, and X-bands) polarimetric scatterometer system capable of making observations every 10 min was developed. This system was used to monitor a soybean field over an entire growth cycle. Measurements of vegetation parameters and VSM were obtained and their relationships to the backscatter observations were examined.

The VV backscatter observations were higher than the HH observations during the initial growth stages (until mid-June). HH observations were higher than VV observations in the later stages of the growth cycle, which was attributed to the increased effect of double bounce. Backscatter coefficients reached their maximum on DOY 271 (corresponding with peak VWC) and then decreased.

Pauli decomposition can provide insight on the relative magnitude of different scattering mechanisms during the soybean growth cycle. We found that double bounce ($\beta$ in Pauli decomposition) was the strongest component for L-band observations. The volume scattering ($\gamma$) was the strongest contribution for X-band observations.

We examined the relationship between the backscattering coefficients of each channel (frequency/polarization) and the various soybean growth parameters. The correlation between the different vegetation parameters and backscatter decreased with increasing frequency. From this analysis, we concluded that L-band HH-polarization is best suited for the monitoring of LAI ($r = 0.98$) and VWC ($r = 0.97$).

This investigation focused on a single incidence angle observing system, in order to improve the quality of the measurements. The angle chosen, 40°, is the same as that chosen by the upcoming SMAP mission. It is expected that the effects of incidence and azimuth angle could affect the results.

These results will be useful in understanding the scattering behaviour of different frequencies in an agricultural field and help in the development of better vegetation and soil moisture retrievals using current and future satellite missions including KOMPSAT-5 COSI (2013), SAOCOM, PALSAR-2, and SMAP (2014).

**Acknowledgements**

This study was funded by the research project (Project No. PJ009367012013) of National Academy of Agricultural Science, Rural Development Administration, Republic of Korea.

**References**

Bouman, B. A. M. 1991. "Crop Parameter Estimation from Ground-Based X-Band (3-Cm Wave) Radar Backscattering Data." *Remote Sensing of Environment* 37: 193–205.

Bouvet, A., and T. Le Toan. 2011. "Use of ENVISAT/ASAR Wide-Swath Data for Timely Rice Field Mapping in the Mekong River Delta." *Remote Sensing of Environment* 115: 1090–1101.

Brakke, T. W., E. T. Kanemasu, J. L. Steiner, F. T. Ulaby, and E. Wilson. 1981. "Microwave Response to Canopy Moisture, Leaf Area Index, and Dry Weight of Wheat, Corn and Sorghum." *Remote Sensing of Environment* 11: 207–220.

Chen, J., H. Lin, and Z. Pei. 2007. "Application of ENVISAT ASAR Data in Mapping Rice Crop Growth in Southern China." *IEEE Geoscience and Remote Sensing Letter* 4: 431–435.

Cloude, S. R., and E. Pottier. 1996. "A Review of Target Decomposition Theorems in Radar Polarimetry." *IEEE Transactions on Geoscience and Remote Sensing* 34: 498–518.

Cuizhen, W., W. Jiaping, Z. Yuan, P. Guangdong, and Q. Jiaguo. 2009. "Characterizing L-Band Scattering of Paddy Rice in Southeast China with Radiative Transfer Model and Multi-Temporal ALOS/PALSAR Imagery." *IEEE Transactions on Geoscience and Remote Sensing* 47: 988–998.

Freeman, M., and S. L. Durden. 1992. "A Three-Component Scattering Model for Polarimetric SAR Data." *IEEE Transactions on Geoscience and Remote Sensing* 36: 356–369.

Inoue, Y., T. Kurosu, H. Maeno, S. Uratsuka, T. Kozu, K. Dabrowka-Zielinska, and J. Qi. 2002. "Season-Long Daily Measurements of Multi-Frequency (Ka, Ku, X, C, and L) and Full-Polarization Backscatter Signatures over Paddy Rice Field and their Relationship with Biological Variables." *Remote Sensing of Environment* 81: 194–204.

Kim, Y. H., S. Y. Hong, and H. Y. Lee. 2009. "Estimation of Paddy Rice Growth Parameters Using L, C, X-Bands Polarimetric Scatterometer." *Korean Journal of Remote Sensing* 25: 31–44.

Kim, Y. H., S. Y. Hong, and H. Y. Lee. 2010. "Construction of X-Band Automatic Radar Scatterometer Measurement System and Monitoring of Rice Growth." *Korean Society of Soil Science and Fertilizer* 43: 374–383.

Kurosu, T., M. Fujita, and K. Chiba. 1997. "The Identification of Rice Fields Using Multi-Temporal ERS-1 C- Band SAR Data." *International Journal of Remote Sensing* 18: 2953–2965.

Lee, J. S., and E. Pottier. 2009. *Polarimetric Radar Imaging: From Basics to Applications*, 280–340. New York: CRC Press.

Maity, S., C. Patnaik, and S. Panigraphy. 2004. "Analysis of Temporal Backscattering of Cotton Crops Using a Semi-Empirical Model." *IEEE Transactions on Geoscience and Remote Sensing* 42: 577–587.

Moran, M. S., A. Vidal, D. Troufleau, Y. Inoue, and T. A. Mitchell. 1998. "Ku- and C-Band SAR for Discriminating Agricultural Crop and Soil Conditions." *IEEE Transactions on Geoscience and Remote Sensing* 36: 265–272.

Oh, Y. S., S. K. Hong, Y. J. Kim, J. Y. Hong, and Y. H. Kim. 2009. "Polarimetric Backscattering Coefficients of Flooded Rice Fields at L- and C-Bands: Measurements, Modeling, and Data Analysis." *IEEE Transactions on Geoscience and Remote Sensing* 47: 2714–2721.

Picard, G., T. Le Toan, and F. Mattia. 2003. "Understanding C-Band Radar Backscatter from Wheat Canopy Using Multiple Scattering Coherent Model." *IEEE Transactions on Geoscience and Remote Sensing* 41: 1583–191.

Pierce, L. E., K. M. Bergen, M. C. Dobison, and F. T. Ulaby. 1998. "Multitemporal Land-Cover Classification Using SIR-C/X-SAR Imagery." *Remote Sensing of Environment* 64: 209–230.

Prasad, R. 2011. "Estimation of Kidney Bean Crop Variables Using Ground-Based Scatterometer Data at 9.89 GHz." *International Journal of Remote Sensing* 32: 31–48.

Prevot, L., M. Dechambre, O. Taconet, D. Vidal-Madjar, M. Normand, and S. Galle. 1993. "Estimating the Characteristics of Vegetation Canopies with Airborne Radar Measurements." *International Journal of Remote Sensing* 14: 2803–2818.

Sarabandi, K., Y. Oh, and F. T. Ulaby. 1992. "Measurement and Calibration of Differential Mueller Matrix of Distributed Targets." *IEEE Transactions on Antennas and Propagation* 40: 1524–1532.

Singh, D. 2006. "Scatterometer Performance with Polarization Discrimination Ratio Approach to Retrieve Crop Soybean Parameter at X-Band." *International Journal of Remote Sensing* 27: 4101–4115.

Ulaby, F. T., C. T. Allen, G. Eger, and E. T. Kanemasu. 1984. "Relating the Microwave Backscattering Coefficient to Leaf Area Index." *Remote Sensing of Environment* 14: 113–133.

Wigneron, J. P., P. Ferrazzoli, A. Olioso, P. Bertuzzi, and A. Chanzy. 1999. "A Simple Approach to Monitor Crop Biomass from C-Band Radar Data." *Remote Sensing of Environment* 69: 179–188.